Journal of Alloys and Compounds 551 (2013) 376–381

Contents lists available at SciVerse ScienceDirect

Journal of Alloys and Compounds

journal homepage: www.elsevier.com/locate/jalcom

Crystallization behavior and hydrogen storage kinetics of amorphous $Mg_{11}Y_2Ni_2$ alloy

Q.A. Zhang *, L.X. Zhang, Q.Q. Wang

School of Materials Science and Engineering, Anhui University of Technology, Maanshan, Anhui 243002, PR China

ARTICLE INFO

Article history:
Received 12 October 2012
Received in revised form 4 November 2012
Accepted 7 November 2012
Available online 16 November 2012

Keywords:
Amorphous Mg-based alloy
Melt-spinning
Crystallization behavior
Hydrogen storage

ABSTRACT

The crystallization behavior and hydrogen storage kinetics of the amorphous $Mg_{11}Y_2Ni_2$ alloy prepared by melt-spinning technique were investigated in detail. It was found that the amorphous $Mg_{11}Y_2Ni_2$ alloy transforms into the crystalline $Mg_{11}Y_2Ni_2$ in metastable state at 279 °C and subsequently decomposes into Mg, $YMgNi_4$ and Y(Mg) solid solution in stable state at 366 °C. All the amorphous, metastable and stable $Mg_{11}Y_2Ni_2$ alloys can be hydrogenated into MgH_2, Mg_2NiH_4 and YH_2/YH_3. However, the stable $Mg_{11}Y_2Ni_2$ alloy has slightly slower hydrogen absorption–desorption kinetics due to the worse dispersivity of YH_2/YH_3 and Mg_2NiH_4.

1. Introduction

Magnesium hydride is a promising material for hydrogen storage because of its high hydrogen capacity and low cost. Nevertheless, the slow kinetics and high temperature of hydrogen desorption prevent MgH_2 from practical applications. To improve the hydrogen absorption–desorption kinetics, many methods such as ball-milling [1,2], hydriding combustion synthesis [3–5], sputtering deposition [6] and doping with nano-sized catalytic additions [7–10] have been used to prepare Mg-based hydrogen storage materials. Comparatively, alloying Mg with Ni or/and rare earth elements is a simple method for accelerating the hydrogen absorption–desorption rate of Mg–H_2 system [11–19].

Recently, Mg–R–Ni (R = rare earth elements) alloys have been intensively investigated because of their high hydrogen capacity and good kinetics [11–26]. The improvement of hydrogen absorption–desorption kinetics can be ascribed to the nano-sized particles of rare earth metal hydrides and Mg_2Ni embedded in Mg matrix [14,15,20–22]. In situ synchrotron X-ray diffraction investigations of hydrogenated Mg–R–Ni samples during their vacuum thermal decomposition processes indicate that the dehydrogenation transformation of MgH_2 to Mg occurs in the presence of $Mg_2NiH_{0.3}$ and rare earth metal hydrides RH_3 or/and RH_2 [12,23–26]. This means that rare earth metal hydrides and $Mg_2NiH_{0.3}$ have a good catalytic effect on the hydrogen absorption–desorption reactions in the Mg–H_2 system. However, the hydrogen storage kinetics is hardly influenced by different rare earth metal hydrides but by the particle size and quantity of the rare earth metal hydrides [15].

Generally speaking, the amorphous Mg–R–Ni alloys prepared by melt-spinning have faster hydrogen absorption–desorption kinetics than the as-cast alloys due to the formation of smaller particle size of rare earth metal hydrides and Mg_2Ni after activation [15,20]. However, it is unclear whether the crystallization of amorphous alloy before activation has an effect on its hydrogen absorption–desorption kinetics. Given that metastable phases are usually formed during the crystallization processes of amorphous Mg–Y–Ni alloys [27,28], $Mg_{11}Y_2Ni_2$ alloy is selected in the present work to understand the effect of crystallization. First, the crystallization behavior of melt-spun $Mg_{11}Y_2Ni_2$ alloy is investigated by annealing at different temperatures. Then, the hydrogenation/dehydrogenation and activation characteristics are also studied. Finally, the hydrogen absorption–desorption kinetic properties of amorphous, metastable and stable alloys are compared in detail.

2. Experimental details

The $Mg_{11}Y_2Ni_2$ alloy was prepared by induction melting of appropriate amounts of a mixture of pure Mg (99.9% purity) and an intermediate YNi alloy under an argon atmosphere (about 0.1 MPa). The as-cast alloy was then re-melted and quenched by melt-spinning with a constant rotating copper roller surface velocity of 40 m/s. The loss of Mg during the induction melting and melt-spinning was determined to be about 18 wt.% by repetitious experiments. On the basis of stoichiometric amounts of starting materials, thus, extra 18 wt.% of Mg was added to compensate the loss of Mg. As a result, the continuously long ribbons with width of about 3 mm and thickness of 30–50 μm were obtained. The melt-spun $Mg_{11}Y_2Ni_2$ alloy obtained was in amorphous state, and its thermal characteristic was studied

* Corresponding author. Tel.: +86 555 2311891; fax: +86 555 2311570.
E-mail address: zhang03jp@yahoo.com.cn (Q.A. Zhang).

0925-8388/$ - see front matter © 2012 Elsevier B.V. All rights reserved.
http://dx.doi.org/10.1016/j.jallcom.2012.11.046

by differential scanning calorimetry (DSC) analysis (Netzsch DSC 404) at a heating rate of 10 °C/min. Based on the DSC result, the melt-spun $Mg_{11}Y_2Ni_2$ alloy was wrapped in a tantalum foil and annealed for crystallization at 300 and 400 °C for 24 h, respectively, under an argon atmosphere (0.6 MPa).

To investigate the hydrogenation and dehydrogenation behavior, the melt-spun and crystallized $Mg_{11}Y_2Ni_2$ alloys were crushed into powders with a size of 300 meshes in a glove box under dry argon atmosphere. The powder samples were loaded into stainless steel containers and then hydrogenated at 300 °C for 1 h under hydrogen pressure of 3.0 MPa and subsequently evacuated for 1 h. After three hydrogenation–dehydrogenation cycles, the samples were fully activated. The hydrogen absorption/desorption kinetics for the activated samples were measured using an automatic Sieverts-type apparatus at 250 °C. Furthermore, the temperature-dependent dehydrogenation curves were also measured using a manual Sieverts-type apparatus.

To evaluate the phase structures of the melt-spun, crystallized and activated samples, powder X-ray diffraction (XRD) measurements were carried out on a Rigaku D/Max 2500VL/PC diffractometer with CuKα radiation at 50 kV and 200 mA. The XRD profiles were analyzed with the Rietveld refinement program RIETAN-2000 [29]. The microstructures of the crystallized samples were observed using a LEO 1530 VP scanning electron microscope (SEM) and a JEM-2010 transmission electron microscope (TEM). The foil samples used for the TEM observations were prepared by the conventional ion milling method.

3. Results and discussion

3.1. Crystallization characteristics

Fig. 1a shows the XRD pattern for the melt-spun $Mg_{11}Y_2Ni_2$ sample. It can be seen that only a hump is present, indicating that it is in an amorphous state. The DSC curve (Fig. 1b) of the melt-spun $Mg_{11}Y_2Ni_2$ alloy shows two exothermic peaks with peak temperatures of 279 and 366 °C, respectively; implying the amorphous $Mg_{11}Y_2Ni_2$ phase undergoes two crystallization steps below 400 °C.

To understand the first crystallization transformation, the melt-spun $Mg_{11}Y_2Ni_2$ alloy was annealed at 300 °C for 24 h and a novel phase was found by XRD pattern. By using the software program TREOR90 [30], the XRD pattern for the novel phase was indexed to be a triclinic unit cell in space group $P\bar{1}$ (No. 2). The crystallographic structure was determined by the software program EXPO [31,32] and further refined by the Rietveld program RIETAN-2000 [29]. As a result, the novel phase is actually a crystalline $Mg_{11}Y_2Ni_2$ phase. Fig. 2a presents the Rietveld refinement of the observed XRD pattern for the $Mg_{11}Y_2Ni_2$ alloy crystallized at 300 °C and the refined pattern fits the observed data points very well. The Rietveld analysis indicates that this sample consists of the crystalline $Mg_{11}Y_2Ni_2$ (96 wt.%), Mg (2 wt.%) and Mg_2Ni (2 wt.%).

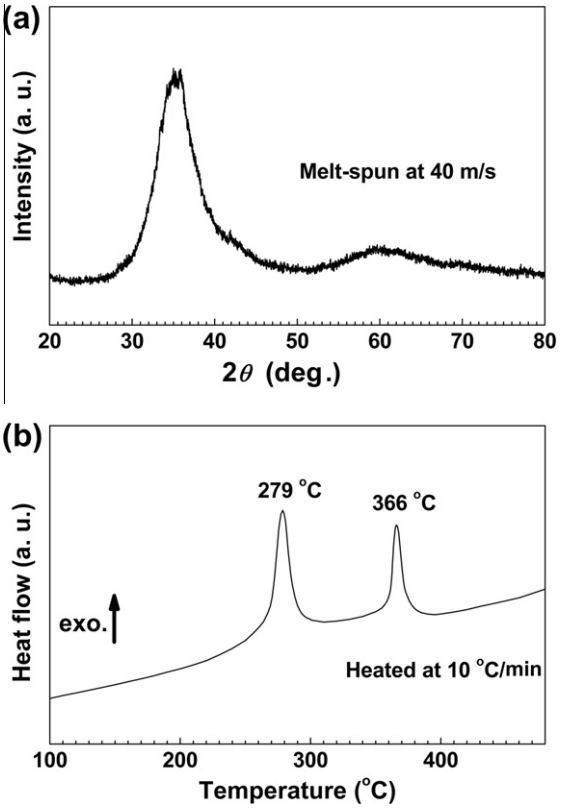

Fig. 1. (a) XRD pattern and (b) DSC curve of the melt-spun $Mg_{11}Y_2Ni_2$ alloy.

The refined structural data of the crystalline $Mg_{11}Y_2Ni_2$ phase are listed in Table 1 and the crystal structure is illustrated in Fig. 2b, which are further confirmed by TEM observation, corresponding selected-area electron diffraction (SAED) pattern and energy dispersive X-ray spectrum (EDS) (see Fig. 3). It can be seen that eleven Mg atoms surround two Y atoms and two Ni atoms in each unit cell. This indicates that the random arrangement of Mg, Y and Ni atoms in the amorphous structure transforms into the segregation of Y and Ni atoms in the crystalline $Mg_{11}Y_2Ni_2$ structure during the first crystallization process. Indeed, the crystalline $Mg_{11}Y_2Ni_2$ is a metastable phase and such segregation offers a preparation for subsequent precipitation in Mg matrix.

Fig. 4a shows the Rietveld refinement of the observed XRD pattern for the $Mg_{11}Y_2Ni_2$ sample crystallized at 400 °C, indicating that this sample is composed of Mg (29 wt.%), $YMgNi_4$ (48 wt.%), Y(Mg) solid solution (13 wt.%) and Y_2O_3 (10 wt.%). The SEM image (see Fig. 4b) clearly shows two types of particles, larger triangles and smaller squares, precipitated in matrix. To distinguish the particles, the microstructures of this sample were investigated by TEM/SAED, as shown in Fig. 5. We find that the triangular particles belong $YMgNi_4$, which has a cubic $SnMgCu_4$ ($AuBe_5$ type) structure [33]. Actually, the square particles were previously found in the solid solution treatment process of Mg–R based alloys and reported as a *f.c.c.* structure with a = 5.6 Å [34–37], but its chemical compo-

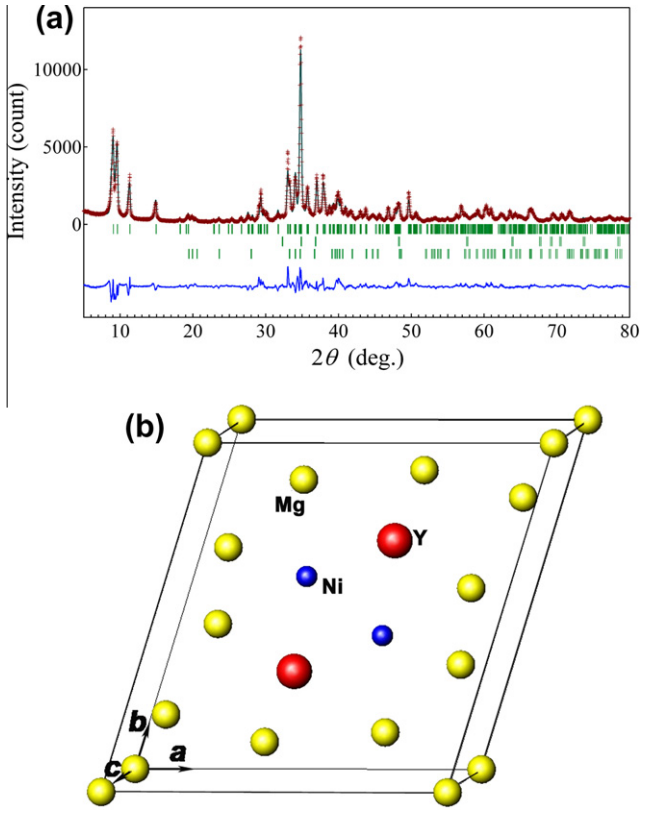

Fig. 2. (a) XRD pattern of the $Mg_{11}Y_2Ni_2$ alloy crystallized at 300 °C, reflection markers (from above) are for the metastable $Mg_{11}Y_2Ni_2$ (96 wt.%), Mg (2 wt.%) and Mg_2Ni (2 wt.%), respectively; and (b) crystal structure of the metastable $Mg_{11}Y_2Ni_2$ phase.